Application of real-time GPS to earthquake early warning in subduction and strike-slip environments

Simona Colombelli,[1,2] Richard M. Allen,[2] and Aldo Zollo [1]

Received 14 December 2012; revised 17 May 2013; accepted 6 June 2013.

[1] We explore the application of GPS data to earthquake early warning and investigate whether the coseismic ground deformation can be used to provide fast and reliable magnitude estimations and ground shaking predictions. We use an algorithm to extract the permanent static offset from GPS displacement time series and invert for the slip distribution on the fault plane, which is discretized into a small number of rectangular patches. We developed a completely "self-adapting" strategy in which the initial fault plane model is built based on a quick, approximate magnitude estimation and is then allowed to increase in size based on the evolutionary magnitude estimation resulting from the slip inversion. Two main early warning outputs are delivered in real-time: magnitude and the along-strike extent of the rupture area. These are finally used to predict the expected ground shaking due to the finite source. We tested the proposed strategy by simulating real-time environments for three earthquakes. For the M_w 9.0, 2011 Tohoku-Oki earthquake, our algorithm provides the first magnitude estimate of 8.2 at 39 s after the origin time and then gradually increases to 8.9 at 120 s. The estimated rupture length remains constant from the outset at ~360 km. For the M_w 8.3, 2003 Tokachi-Oki earthquake, the initial magnitude estimate is 8.5 at 24 s and drops to 8.2 at 40 s with a rupture length of 290 km. Finally, for the M_w 7.2, 2010 El Mayor-Cucapah earthquake, the magnitude estimate is 7.0 from the outset with a rupture length of 140 km. The accuracy of the ground shaking prediction using the GPS-based magnitude and finite extent is significantly better than existing seismology-based point source approaches. This approach would also facilitate more rapid tsunami warnings.

Citation: Colombelli, S., R. M. Allen, and A. Zollo (2013), Application of real-time GPS to earthquake early warning in subduction and strike-slip environments, *J. Geophys. Res. Solid Earth*, *118*, doi:10.1002/jgrb.50242.

1. Introduction

[2] The combined use of seismic and geodetic observations is now a common practice for finite fault modeling and seismic source parameterization. With the advent of high-rate 1 Hz GPS stations, the seismological community has recently begun looking at GPS data as a valid complement to the seismic-based methodologies for Earthquake Early Warning (EEW).

[3] In the standard approaches to EEW, the initial portion of the *P* wave signal is used to rapidly characterize the earthquake magnitude and to predict the expected ground shaking at target sites, before the arrival of the most damaging waves. Different EEW parameters (such as the initial peak ground displacement and period parameters) are measured in a 3–4 s *P* wave time window. They are used to get independent estimates of the earthquake magnitude and to predict the following peak ground motion at the recording site. Based on the analysis of strong motion records, empirical scaling relationships between EEW parameters and earthquake size have been derived [*Allen and Kanamori*, 2003; *Kanamori*, 2005; *Zollo et al*., 2006; *Wu and Zhao*, 2006; *Böse et al*., 2007; *Wu and Kanamori*, 2008; *Shieh et al*., 2008] and are implemented or being tested in many active seismic regions of world. Operational Earthquake Early Warning Systems are currently running in Japan [*Nakamura*, 1984, 1988; *Odaka et al*., 2003; *Horiuchi et al*., 2005], Taiwan [*Wu and Teng*, 2002; *Wu and Zhao*, 2006], and Mexico [*Espinosa-Aranda et al*., 2009], while other systems are under testing or development in California [*Allen et al*., 2009a; *Allen et al*., 2009b; *Böse et al*., 2009], Turkey [*Alcik et al*., 2009], Romania [*Böse et al*., 2007], China [*Peng et al*., 2011], and Southern Italy [*Zollo et al*., 2009; *Satriano et al*., 2010; *Zollo et al*., 2013]. Whether the final magnitude of an earthquake can be predicted while the rupture process is underway remains a controversial issue. However, the limitations of the standard approaches when applied to giant earthquakes have become evident after the experience of the M_w 9.0, 2011 Tohoku-Oki earthquake.

Additional supporting information may be found in the online version of this article

[1]Dipartimento di Scienze Fisiche, Università di Napoli Federico II, Naples, Italy.
[2]Berkeley Seismological Laboratory, University of California, Berkeley, California, USA.

Corresponding author: S. Colombelli, Department of Physics, University of Naples "Federico II" Complesso Universitario di Monte S. Angelo, Via Cintia, IT-80126 Naples, Italy. (simona.colombelli@unina.it)

2169-9313/13/10.1002/jgrb.50242

[4] One limitation is that, because EEW systems are essentially applied to moderate to strong earthquakes, large dynamic range, accelerometric sensors are generally used for real-time seismic applications. These instruments are able to record unsaturated signals without risk of clipping at the arrival of the strongest shaking. Accelerometer waveforms are usually integrated twice to obtain displacement time series; for near-field records, this operation may lead to unstable results. Precise recovery of ground displacement requires accurate baseline corrections and estimations of rotation and tilt motion [*Kinoshita and Takagishi*, 2011]. For real-time purposes, a high-pass causal Butterworth filter is generally applied to remove the artificial effects and the long-period drifts introduced by the double integration operation [*Boore et al*., 2002]. The application of the high-pass filter, while removing the artificial distortions, reduces the low-frequency content of the recorded waveforms, resulting in the complete loss of the low-frequency energy radiated by the source and of the static offset. This effect is even more relevant for very large earthquakes, whose corner frequency is expected to be lower or comparable with the cutoff filtering frequency (typically 0.075 Hz). Since GPS stations are able to register directly the ground displacement without any risk of saturating and any need of complicated corrections, geodetic displacement time series represent an important complementary contribution to the high-frequency information provided by seismic data.

[5] Broadband velocity seismometers are currently well distributed around the globe and might represent an alternative to accelerometric sensors, since one single integration operation would be needed to retrieve the displacement waveform. An important limitation to the use of broadband velocity seismometers is that these instruments will saturate at relatively short distances from the source during the occurrence of large earthquakes, i.e., when our methodology is most useful, while accelerometric sensors are able to record unsaturated signals without risk of clipping at the arrival of the strongest shaking. Moreover, the velocimeter instrument response is not flat a low frequencies, and this does not allow the complete retrieval of ground motion frequency content.

[6] Another relevant limitation of the seismic methodologies is the saturation effect of EEW parameters for large magnitudes ($M > 7.5$–8) [*Kanamori*, 2005; *Rydelek and Horiuchi*, 2006; *Rydelek et al*., 2007; *Zollo et al*., 2007; *Brown et al*., 2009]. Although the rupture process of large earthquakes is not yet fully understood, the saturation is likely due to the use of a limited portion of the *P* wave signal which is not enough to characterize such a large time/space scale phenomena. In real-time approaches, the possibility of progressively expanding the observation time window throughout the whole record while the event is evolving allows capture of longer portions of the rupture process and lower frequencies radiated from the source. GPS methods provide the evolutionary measurement of a ground motion quantity which is directly related to the earthquake magnitude; the permanent ground deformation, i.e., the resulting coseismic displacement after the dynamic vibration has finished, is generally used to estimate the earthquake magnitude from GPS data.

[7] The challenge with GPS data is therefore a practical one, being related to the development of real-time methodologies to retrieve, process, and analyze geodetic displacement time series. The main limitation of GPS data is that the coseismic ground displacement starts to be evident later than the *P* wave arrival on the seismic records and approximately at the same time of the *S* wave arrival [*Allen and Ziv*, 2011]. However, this does not prevent the use of close-in GPS stations for the issuance of a warning with the expected ground shaking at more distant sites and for the use of these data for tsunami early warning. Minor limitations to the use of real-time GPS data can be related to baseline and satellite ephemeris errors. However, several studies have already demonstrated that instantaneous, single epoch positioning using ultrarapid orbits yields precisions on the order of a few centimeters [*Yamagiwa et al*., 2006; *Genrich and Bock*, 2006], while offsets on the order of tens of centimeters are expected in the context of early warning applications. In the ideal approach to EEW, seismic and GPS data should be used sequentially: as soon as seismic methodologies run into their limitations due to saturation, GPS data can provide information with a high signal-to-noise ratio, confirming and/or upgrading the information previously released using seismic methods.

[8] Many authors have recently started applying GPS data to EEW [*Allen and Ziv*, 2011; *Crowell et al*., 2012; *Wright et al*., 2012; *Ohta et al*., 2012]; they show that a rapid and remarkably robust magnitude estimate can be obtained, while the rupture process is underway. Here we investigate whether and how 1 Hz GPS data can be used for both the rapid determination of the event size and for the real-time estimation of the rupture area, which would allow for a better prediction of the expected ground shaking at the target sites. For a practical implementation of EEW systems, rapidity and reliability of the real-time estimations are fundamental features for the diffusion of a warning and for the decision-making processes of the nonexpert, end-user audience. Thus, we focus our efforts on the development of a rapid, stable, but approximate methodology and let more complex, postevent analysis achieve a complete and refined fault model characterization.

2. Data

[9] For the present work, we analyzed the real-time 1 Hz GPS data collected during three earthquakes: the M_w 9.0 2011 Tohoku-Oki earthquake, the M_w 8.3 2003 Tokachi-Oki earthquake, and the M_w 7.2 2010 El Mayor-Cucapah earthquake. The difference in magnitude, location, and source mechanism makes these three events an ideal data set to test the proposed methodology.

[10] For the 2011 Tohoku-Oki earthquake, raw 1 Hz GPS data were collected by the Japanese GPS Earth Observation Network (GEONET) stations [*Sagiya*, 2004]. Point positions were provided by the Pacific Northwest Geodetic Array at Central Washington University and were computed using GPS Inventory Modeling and Monitoring Study (GIPSY 6) and final satellite ephemerides and clock corrections provided by the Jet Propulsion Laboratory. For the 2003 Tokachi-Oki earthquake and the 2010 El Mayor-Cucapah earthquake, the raw 1 Hz GPS data were collected by GEONET and California Real-Time Network (CRTN) stations, respectively. Both data sets are the same used by *Crowell et al*. [2012]. These data were postprocessed using the method of instantaneous positioning described in *Bock et al*. [2011]. *Langbein and Bock* [2004] reported that, for 1 Hz GPS data, the scatter of the vertical component is about

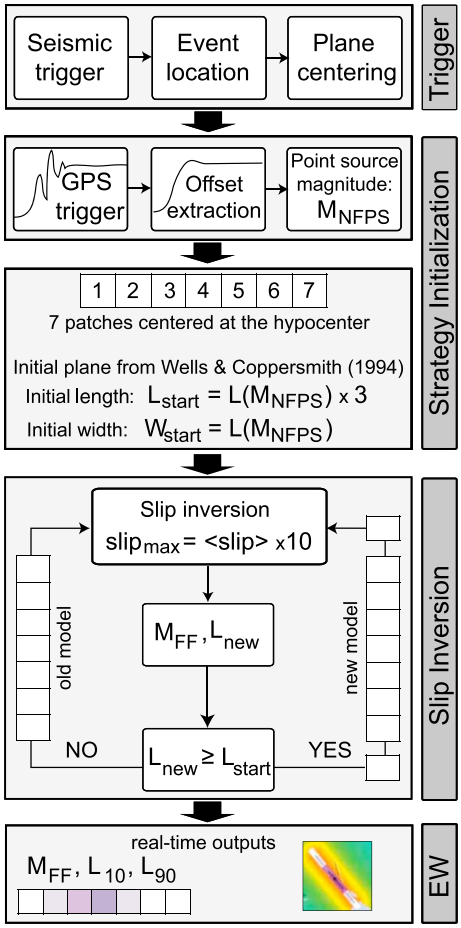

Figure 1. Flowchart illustrating the inversion strategy. Once the seismic network triggers on an earthquake, the algorithm monitors for a trigger on the GPS displacement time series at which point it starts the offset extraction. A rapid estimation of magnitude (M_{NFPS}) is obtained from the first available offset (~10 s after the first trigger) using the near-field, point source approximation and is used to define the size of the initial fault plane model. The expected length and width are computed from *Wells and Coppersmith* [1994] scaling relationships. The starting length (L_{start}) is assumed to be 3 times the expected value based on magnitude. This fault plane is then divided into seven equal patches, oriented based on a catalog of faults, and positioned to intersect the seismically defined hypocenter. For the first slip inversion, the allowed range of slip on each patch is also based on M_{NFPS}. The maximum allowed slip is 10 times the expected slip, as computed from M_{NFPS} and the fault plane area. The slip inversion is then repeated every second. Following each inversion, the new magnitude (M_{FF}) is used to estimate an expected fault length (L_{new}). L_{new} is then compared to L_{start}. If L_{new} is smaller than L_{start}, the same model is adopted, and a new inversion is run. If L_{new} is greater than L_{start}, the fault plane length is increased, and two patches are added at each end of the fault. At each time step, the allowed slip range on each patch is set to 0 to 3 times the slip recovered from the previous inversion. Three real-time outputs are provided by the inversion strategy at each time: the current magnitude estimate resulting from the slip inversion (M_{FF}), and the real-time estimations of L_{10} and L_{90}. M_{FF} and L_{10} are finally used to predict the ground shaking in the region.

5 times larger than that of the horizontal components. The estimated real-time average error is approximately 5 mm for the horizontal components and 10 mm for the vertical one. The time series used in this study are postprocessed products that utilize the refined orbit and clock corrections. The actual real-time series would likely have higher uncertainties and might lead to greater fluctuations in the estimated magnitude, especially at the early stage of the inversion process when few data are used. For the purpose of this study, we focus on the best way to analyze the displacement time series and on the rapid extraction of source parameters in real-time rather than on the methodologies used to process the real-time GPS data.

3. GPS Methodology

[11] Following the approach proposed by *Allen and Ziv* [2011], we developed an efficient real-time static slip inversion scheme to provide a reliable magnitude estimate and a rapid estimation of the rupture area extent. We do not attempt to solve for detailed slip models, but our focus here is to maximize the stability of the methodology when only limited information about the ongoing earthquake is available. The strategy we propose is simple and robust and is expected to be suitable for any seismically active region since it does not require restrictive prior assumptions. An intrinsic limitation of the methodology is related to the sensitivity of GPS sensors and to their ability to detect seismic signals above the noise level. Several authors have shown that for large earthquakes ($M > 7$), 1 Hz GPS data can be successfully used to detect waves [*Larson et al*., 2003; *Bock et al*., 2004]. For the M_w 6.3, 2009 L'Aquila earthquake, significant ground deformations (> 10 cm) have been found within a radius of 60 km from the epicenter, and 1 Hz GPS data have been successfully applied to estimate magnitude, extension of the seismic source, and details about the rupture process [*Anzidei et al*., 2009; *Cirella et al*., 2009; *Avallone et al*., 2011]. A magnitude of about 6.0–6.5 is expected to be the lower threshold for the application of the proposed GPS-based strategy for EEW. The main steps of the strategy are described in the flowchart diagram (Figure 1), and a detailed description for each step is given in the following sections.

3.1. Permanent Displacement Extraction

[12] The preliminary step for the inversion strategy is the real-time extraction of the static offset (Figure 1). The permanent deformation is mathematically described by the near-field term in the Green's function. Due to its rapid decay with distance (as $1/R^2$) [*Aki and Richards*, 2002; *Kanamori and Brodsky*, 2004], the static deformation can be dominant in the proximity of the source but is generally obscured by the dynamic component at greater distances. Although accurate estimates of the permanent displacement can be easily obtained in the postevent phase, following dynamic motion, the static deformation is expected to arrive shortly after the arrival of the first dynamic component. As long as we are able to distinguish the static component from the dynamic oscillation, real-time estimations of the permanent ground deformation can be achieved before the dynamic component has subsided.

[13] In order to extract the static component, we used the algorithm developed by *Allen and Ziv* [2011]. The algorithm

looks for a trigger along the record using a predetermined condition on the short-term signal average (STA) versus long-term signal average (LTA) [*Allen*, 1978]. For all the analyzed earthquakes, the short-term and the long-term time windows have been set to 2 and 100 s, respectively, and the STA/LTA threshold ratio for the triggering declaration has been set to 10. These values have been found by trial and error to provide correct trigger attributions at close-in stations and to avoid false triggers at distant sites. Starting from the trigger time, a cumulative running average of the observed displacement is computed along the waveforms and is delivered as a real-time estimation of the static offset. To prevent the inappropriate use of a dynamic oscillation amplitude as the permanent offset, the algorithm starts to deliver the running average after (a) two zero crossings, (b) two trigger-amplitude crossings, or (c) 10 s after the trigger time, whichever comes first. These three conditions have been purposely designed to account either for cases where the dynamic oscillation is dominant (and the signal is a sinusoidal-type oscillation) or for cases where the static component is dominant (and the waveform is a ramp-type signal). Use of the running average as an estimate of the static offset is expected to remove, or reduce, the contribution of the dynamic component of the signal, which would affect the estimation of the static offset. The use of longer time windows for averaging would stabilize the static offset estimation, but they would also delay the final solution. Various approaches for the real-time offset extraction have been proposed based on moving average windows with different length. Among them, after looking at their performance in terms of delivery time and stability of the static offset for all stations for these three earthquakes, we find the algorithm proposed by *Allen and Ziv* [2011] to be the most general and efficient approach. Because of the logarithmic scaling between the permanent deformation and magnitude (through the seismic moment), once the dynamic component has been carefully removed, further small variations in the static offset due to noise or spurious signal contaminations do not have a significant effect on the magnitude estimate.

3.2. Point Source Magnitude

[14] As soon as the static offset estimate is available at the first triggered GPS station, a preliminary estimation of the earthquake size can be obtained by approximating the source as a point source and assuming a short source-receiver distance. A point dislocation is obviously an unrealistic model for big earthquakes recorded at near-source distances, but this assumption may provide a useful and rapid initial magnitude estimate from the early recorded signals. At short distances from the source, the primary component of the static displacement, u, can be written as [*Aki and Richards*, 2002; *Kanamori and Brodsky*, 2004]:

$$u = \frac{1}{4\pi\mu R^2} M_0 \tag{1}$$

where μ is the rigidity modulus of the medium, R is the hypocentral distance, and M_0 is the seismic moment. The application of this formula requires the earthquake hypocenter to be known. Although reliable trigger techniques for GPS data have been proposed [e.g., *Ohta et al.*, 2012], real-time algorithms for earthquake detection on seismic records are more accurate and long proven and are able to provide reliable estimates of the earthquake location within few seconds from the first P wave detection [*Satriano et al.*, 2008]. While accurate locations are not required for this preliminary magnitude estimation, the contribution of seismic EEW methodologies is obviously essential for this stage of our GPS-based strategy. The preliminary near-field, point source magnitude (hereafter M_{NFPS}) is useful in its own right and provides a better estimate of magnitude than seismic-based EEW methodologies alone (see later examples). In addition, the M_{NFPS} estimate and the seismic-based hypocenter location are then used to initialize the inversion scheme, i.e., to determine the initial fault plane to be used for the first real-time static slip inversion, according to the procedure discussed below.

3.3. Static Slip Inversion

[15] The slip inversion step starts with the construction of the initial fault plane geometry; two pieces of information are required. The first is the position (geographical coordinates) and the orientation (strike, dip, and rake) of the fault plane. Various catalogs of active faults around the world have been compiled and provide position, geometry, and orientation. This is true for the plate boundary faults, including the major subduction zones that are part of this study, and also for regional faults in California and Mexico. In our approach, we make the assumption that the orientation of the fault plane is that of the nearest known fault plane, as taken from the appropriate regional fault catalog. We then locate the fault plane, with an orientation based on the nearest know fault, such that it intersects the hypocenter for the event underway. The second necessary piece of information is a rough estimation of the fault plane extent along the strike and the dip directions. An approximate but reasonable fault plane model is fundamental both to avoid initial over/underestimations, which may bias the following solutions, and to ensure minimal computation times and maximal resolution of the slip distribution. The near-field, point source magnitude is a reasonable starting value to set up the size of the initial fault plane model.

[16] The size of the fault plane model is determined using the empirical scaling relationships from *Wells and Coppersmith* [1994] relating the earthquake magnitude to the surface rupture length and the downdip rupture length [*Wells and Coppersmith*, 1994, Table 2A]. We use the appropriate scaling relationship for each specific tectonic environment (i.e., for normal, reverse, or strike-slip ruptures). Furthermore, to account for bilateral ruptures, and to accommodate the uncertainties in the scaling relationships and the real-time magnitude estimates, our parameterized model has a fault length 3 times the length provided by the scaling relation along strike. For simplicity and to minimize the computational time, we initially discretize the fault plane into seven rectangular, equally sized rupture segments, all of which extend the full downdip width of the fault. Our target is an approximate estimation of the along-strike extension of the rupture (i.e., the length of a line source). This model setup allows the lateral extent of the slip to vary, and therefore to be determined, in both directions from the hypocenter, neglecting the downdip variations of slip distribution. We found that 7 is a reasonable number of patches as it allows for a sufficient slip variability along the strike of a $M > 6$ earthquake fault in just one or both rupture directions while also keeping the model parameters to a minimum. Having a fixed

number of patches clearly affects the spatial resolution of the slip model and does not allow capture of slip heterogeneity smaller than the size of the patches themselves. Again, for the aim of our methodology, a rather accurate reconstruction of the slip model is not required.

[17] The inversion starts as soon as the first estimation of the static offset at the first triggered station is available. The offset estimates are updated every second (the data is one sample per second), and the slip distribution is therefore recalculated every second as new data become available. We model the static offset (both horizontal and vertical) using the rectangular dislocations along our defined fault plane embedded in a homogenous half-space. The entire fault plane is discretized into independent subfaults, and the slip on each patch is assumed to be constant [*Okada*, 1985]. The general problem of inversion for slip is nonlinear since surface displacements are nonlinear functions of the fault geometry through the analytic expression of the Green's functions derived by *Okada* [1985]. However, when fault geometry and orientation are fixed, the inverse problem becomes linear and can be written as:

$$\mathbf{Gm} = \mathbf{d} \tag{2}$$

where **G** is the matrix of Green's functions relating the model parameter **m** (slip on each patch) to the observed permanent ground displacement **d**. We solved for the slip on each patch by minimizing the square misfit (L2 norm) between observed and predicted displacements. To regularize the inversion, the slip is constrained to a single direction. For subduction zones, only solutions with normal dip slip are permitted, and in translational tectonic environments, only lateral strike-slip is allowed. To avoid rough slip distributions, we applied a median filter to smooth the solution and impose the slip to taper to zero at the edge of the fault.

[18] We solve the inverse problem through a genetic algorithm [*Holland*, 1975, 1992] implemented in a MATLAB code [*Shirzaei and Walter*, 2009]. Although the platform chosen is not the most appropriate for real-time operations, the optimization of the algorithm would require a complete rewriting of the code, and this goes beyond the purpose of the present study. For the first inversion, we explore any possible slip value in a range which is determined from M_{NFPS}. Given the fault plane area and the initial seismic moment, we compute the corresponding average slip value (through the definition of seismic moment) and set an initial exploration range around this value. For the specific case of our algorithm, the initial exploration range was set from 0 to 10 times the average slip value. After the first inversion, to stabilize and speed up the estimation of the slip distribution, we constrain the genetic algorithm to look for the optimal solution in a range that is determined based on the results of the previous inversion. At each inversion run following the first one, the slip on each patch is allowed to vary in a narrow range around the value of the previous inversion (0 to 3 times the maximum slip). This range has been found by trial and error to guarantee the stability of the solution at each time, without restricting the exploration range excessively. Given the slip distribution, the corresponding seismic moment is computed by multiplying the integral of the slip over the fault area by the shear modulus (here assumed to be 33 GPa). The moment magnitude is finally obtained through the moment-magnitude relationship of *Hanks and Kanamori* [1979].

3.4. Ground Shaking Prediction

[19] The evolutionary magnitude estimate resulting from the slip inversion is finally used to predict the intensity distribution in the proximity of and far away from the source. The Peak Ground Acceleration (PGA) and Peak Ground Velocity (PGV) are first predicted using a standard ground motion prediction equation relating magnitude, distance, and the ground motion quantities. The instrumental intensity is then obtained from PGA and PGV using an empirical conversion relationship.

[20] For El Mayor-Cucapah earthquake, we follow the approach used by ShakeMap (U.S. Geological Survey, USGS). We compute the expected PGA and PGV using the ground motion estimation equation of *Boore et al*. [1997], which has the form:

$$\begin{aligned} 1nY = b_1 + b_2(M-6) + b_3(M-6)^2 \\ + b_5 1n\sqrt{r_{\mathrm{jb}}{}^2 + h^2} + b_v 1n(v_s/v_a) \end{aligned}$$

where M is the magnitude, v_s is the average shear wave velocity (upper 30 m), r_{jb} is the Joyner-Boore distance (distance from the surface projection of the fault plane) [*Joyner and Boore*, 1981] and b_1, b_2, b_3, b_5, b_v, v_a, and h are parameters derived from the regression. For the $b1$ coefficient, we assumed the strike-slip source type. PGA and PGV are then converted into a Modified Mercalli Intensity (MMI) scale, using the empirical relationship of *Worden et al*. [2012]:

$$\begin{aligned} \mathrm{MMI} &= c_1 + c_2 \log(Y) \quad \text{for } \log(Y) \le t_1 \\ \mathrm{MMI} &= c_3 + \mathrm{c}_4 \log(Y) \quad \text{for } \log(Y) > t_1 \end{aligned}$$

where Y is the ground motion quantity (PGA or PGV) and c_1, c_2, c_3, c_4, and t_1 are coefficients derived from the regression.

[21] For the Japanese earthquakes, we followed the approach of the Japan Meteorological Agency (JMA) to compute the expected seismic JMA intensity (I_{JMA}) at each site. We first compute the expected PGV distribution using the attenuation relationship of *Si and Midorikawa* [1999], which is written as:

$$\log A = aM + hD + d + e - \log(R + c) - kR$$

where A is the ground motion parameter (PGA or PGV), M is the magnitude, D is the source depth, R is the distance from the fault plane, and a, c, d, e, h, and k are coefficients resulting from the regression analysis. PGV is then converted into a seismic intensity value using the relationship of *Midorikawa et al*. [1999]:

$$I_{\mathrm{JMA}} = p + q \log(\mathrm{A}) \quad 4 \le I_{\mathrm{JMA}} \le 7$$

where A is the ground motion quantity (PGV), and p and q are parameters derived from the regression.

[22] For both the El Mayor-Cucapah earthquake and for the Japanese events, we assumed a rock-soil type and did not consider any amplification/attenuation effect due to local site conditions.

3.5. Real-Time Strategy and Early Warning Outputs

[23] We start the inversion strategy using the initial fault model dimensions as estimated based on *Wells and Coppersmith* [1994] relationships and dividing the entire fault plane into seven rectangular patches. Given that the initial size of the model fault plane is determined based on the first magnitude estimate using the near-field point source approximation (M_{NFPS}), it is important to allow the fault plane to increase in size. We use a "self-adapting" strategy in which the fault plane can increase in size based on the evolutionary magnitude estimation (Figure 1). At each inversion, the current magnitude value is used to compute the corresponding length (the expected length from *Wells and Coppersmith* [1994]). As soon as the new estimated length exceeds the initial value, the model is upgraded. This is done by resizing the entire fault plane (in both length and width) and adding two additional fault patches, one at each end of the plane. Adding two extra patches when the plane needs to be expanded maintains consistency with the previous model in terms of slip distribution and ensures an approximately constant spatial slip resolution over time. For the two new extreme patches, we assume the same initial slip range as for the inner adjacent patch.

[24] Two main pieces of information are released in real-time as output from the inversion algorithm: the magnitude (finite fault magnitude, hereafter M_{FF}) and the rupture area extent. We characterize the rupture extent in terms of rupture length along strike and centroid location. We determine where along the fault the slip amplitude drops to 90% and 10% of the maximum value using a piecewise linear fit to the slip values of each patch. We refer to these lengths as L_{90} and L_{10}, respectively.

[25] The real-time measures of magnitude and rupture area length are finally used to produce the expected ground shaking distribution due to the extended finite source. We followed the methodology described in section 3.4 using, at each 1 s iteration, the current magnitude value and the L_{10} estimate as a measure of the fault plane length. The fault plane width is fixed at the same value as used for the slip inversion, and for the shaking prediction, the plane is centered on the middle point of L_{10}. The expected intensity distribution is thus computed based on distance from the finite fault.

4. Application and Results

[26] We applied the proposed methodology to the three selected events. We do this in a simulated real-time environment and also assume that the real-time implementation benefits from some basic information from seismic-based EEW systems. Specifically, we assume that *P* wave triggers at the closest seismic sites provide an earthquake hypocenter. This hypocenter is used to position the model fault plane (the plane is centered at the hypocenter) and also to determine the expected *P* wave arrival time at each GPS station. Estimates of the static offset from GPS records are only used following the predicted *P* wave arrival. Note that the GPS time series also has to trigger in order to provide static offset estimates (see section 3.1). Furthermore, to prevent small noise oscillations in the displacement data far from the source from leading to widespread, flat, slip distributions, we applied a threshold condition on the horizontal motion, following the approach of *Crowell et al.* [2012]. At each station, the static offset is only used when the horizontal motion is more that 15 mm, which is about 3 times the expected one-sigma precision for single epoch instantaneous GPS positioning on the horizontal components [*Langbein and Bock*, 2004].

[27] To evaluate the performance of the ground shaking prediction, we compared predicted and observed intensity distributions. We computed the intensity distribution for two different cases: (a) using the real-time magnitude estimate and the distance from a point source (hypocenter) and (b) using the real-time magnitude estimate and the distance from the finite fault plane (with L_{10} as a measure of the fault plane length). For each analyzed event, we quantify the difference at each time through the root-mean-square (RMS) residual between the real (observed) intensity and the real-time predicted value at any point of the considered area.

4.1. The M_w 9.0 2011 Tohoku-Oki Earthquake

[28] The M_w 9.0 2011 Tohoku-Oki earthquake occurred on 11 March at 05:46:24 UTC offshore of the northeast coast of Honshu, Japan, on the subduction boundary between the Pacific and the North American plates. The USGS's W-phase moment tensor inversion and finite fault model solutions suggest a megathrust earthquake (strike 193°, dip 14°, and rake 81°) rupturing an area of approximately 300×150 km with a cumulative seismic moment of 4.42×10^{22} Nm. Coseismic, postevent slip models indicate that the fault moved upward of 30–40 m with a permanent horizontal displacement exceeding 4 m at the closest coastal station and significant ground motion up to 300 km from the hypocenter [*Simons et al.*, 2011]. We analyzed the coseismic ground deformations collected by 847 3 component recording stations of the Japanese GPS Earth Observation Network (GEONET) [*Sagiya*, 2004], in a distance range between 120 and 600 km from the hypocenter. We use a subduction interface with strike and dip of 195° and 15°, respectively, based on the USGS National Earthquake Information Center catalog of subduction zone plate boundaries (http://earthquake.usgs.gov/research/data/slab/). We position the fault plane to intersect the earthquake hypocenter, and we assume a pure reverse fault mechanism.

[29] The GPS-trigger algorithm declares the first arrival at the closest station (station 0550, along the Sendai coast) 29 s after the earthquake origin time and starts to deliver the running estimate of the static displacement 10 s later. At the same time, the magnitude estimation with the near-field and point source approximation gives $M_{NFPS} = 8.22$. With this magnitude, we build our starting model with seven rectangular patches of 90×50 km each (for total dimension along strike of 630 km, i.e., 3 times the expected length) and proceed with the slip inversion step. In the case of this earthquake, although the magnitude estimate increases, the corresponding estimated length does not exceed the length of starting model; the increase in size of the fault plane is thus never triggered. At each time, the current magnitude value and the length estimation are used to predict the expected ground shaking distribution, assuming the corresponding finite fault plane, as explained before. Figure 2 summarizes the results of our strategy for three different times [39 s (Figure 2d), 100 s (Figure 2e), and 200 s (Figure 2f)]. The entire evolution with time is shown in Figure S1 in the supporting information.

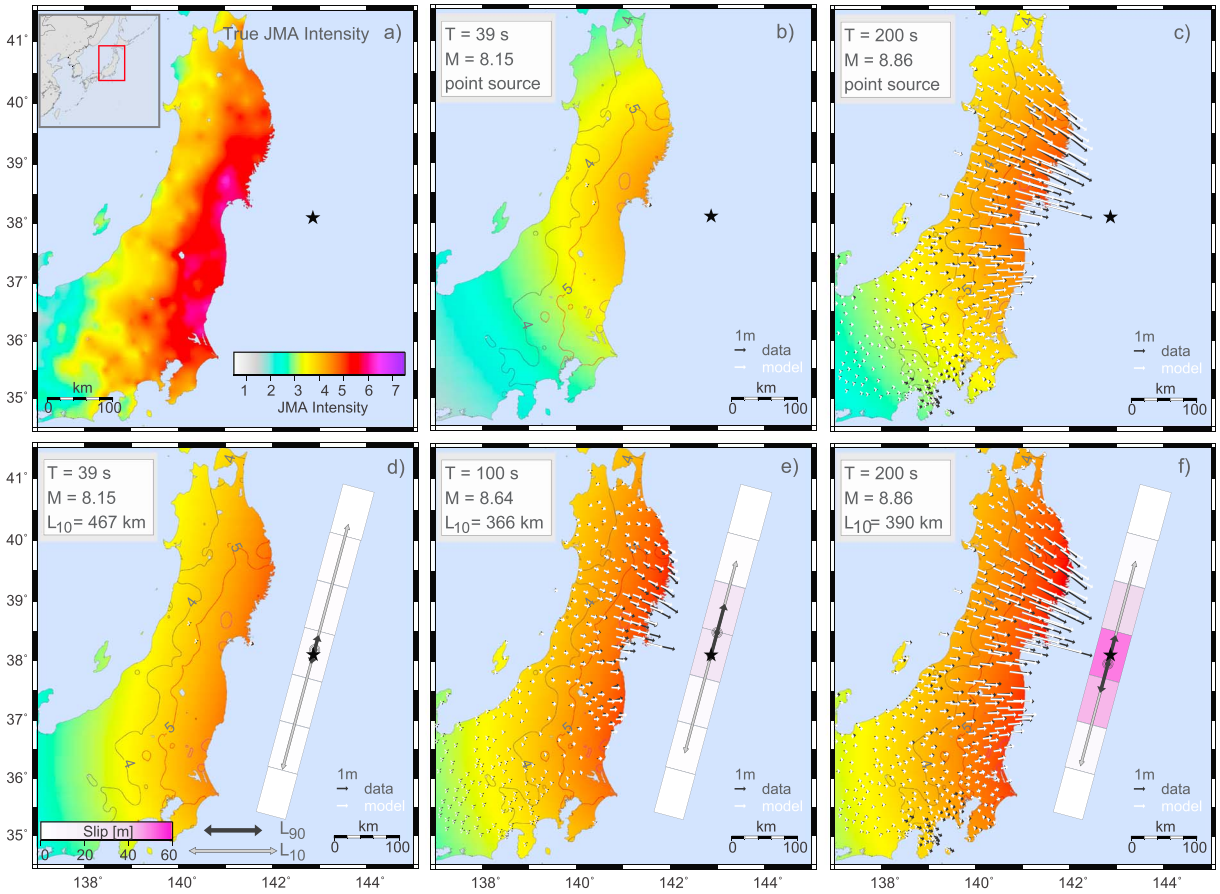

Figure 2. Snapshots of the GPS-based strategy for the M_w 9.0, 2011 Tohoku-Oki earthquake at three different times comparing the intensity prediction using the point source and the finite fault. (a) The true JMA intensity distribution. (b and c) The ground shaking predictions (background color scale) assuming a point source (at the hypocenter) at 39s (Figure 2b) and at 200 s (Figure 2c), respectively. (d, e, and f) The results of the finite source strategy obtained at 39s (Figure 2d), 100 s (Figure 2e), and 200s (Figure 2f). The background color here represents the predicted intensity distribution using the current magnitude value and the distance from the finite fault (L_{10}). The purple color scale shows the slip distribution on the seven-patch slip model. The length estimates L_{10} and L_{90} are also plotted as vectors on the fault plane with a narrow gray vector, and a thick, shortest black vector, respectively. The current value of L_{10} is displayed in the gray box. The small circles at the center of the L_{90} segment correspond to the midpoint that we use as the centroid of the maximum slip area. In each panel from Figures 2b to 2f, black vectors represent the observed horizontal offset while white vectors show the static displacement resulting from the inversion algorithm. The gray and red foreground lines represent the JMA = 4 and JMA = 5 contour lines, respectively. The current time and magnitude value are also displayed in the gray box.

[30] For this earthquake, our real-time magnitude estimation (Figure 3a) is extremely robust and consistent with that of other simulated real-time analysis [*Wright et al.*, 2012; *Ohta et al.*, 2012]. Both magnitude estimations (M_{NFPS} and M_{FF}) show a similar behavior. The first estimation is available at 39 s after the origin time, when M_{NFPS} is 8.23 and M_{FF} is 8.15. The two magnitudes rapidly increase reaching a first plateau level around 60 s, when M_{NFPS} gives 8.5 and M_{FF} gives 8.4. A new increase begins around 80–90 s, and both magnitudes reach their near-final values ($M_{NFPS} = M_{FF} = 8.9$) around 120 s.

[31] Stable estimates of both L_{10} and L_{90} result from the slip inversion as well. L_{10} (intended to represent the total length of the rupture) ranges from 298 to 476 km, with a mean value of 360 ± 30 km over the entire time period. L_{90} (length of peak rupture) varies between 30 and 199 km, with a mean value of 83 ± 42 km (Figure 3b). Several authors have derived coseismic slip distributions and finite fault models for the M_w 9.0, 2011 Tohoku-Oki earthquake using a variety of data sets (*Iinuma et al.* [2011], *Lee et al.* [2011], *Romano et al.* [2012], and *Suzuki et al.* [2011], among many others). The fault plane is usually modeled as a rectangular area of approximately 400 × 200 km. A common result between all these models is the presence of extremely large slip asperity (with slip greater than 50 m) concentrated around the hypocenter in a relatively small area (about 100 × 40 km). A qualitative, visual comparison of our real-time results with postevent analysis shows that L_{10} provides a good estimation of the total ruptured area and L_{90} is consistent in both position and extension with the largest observed asperity.

[32] The RMS plot of Figure 3c shows the difference between predicted and observed intensity at each time. We

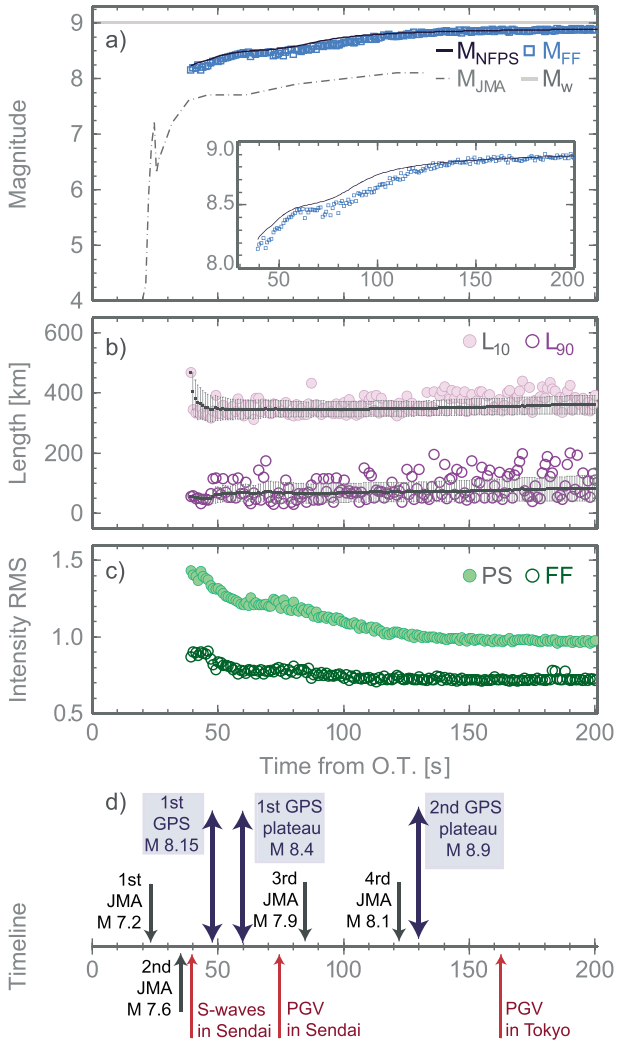

Figure 3. Real-time output for the M_w 9.0, 2011 Tohoku-Oki earthquake. Results of the inversion strategy as a function of time from the origin time. (a) Magnitude with the near-field, point source approximation (M_{NFPS}—dark blue solid line) and magnitude resulting from the slip inversion (M_{FF}—small blue squares) (a zoom of the curves is shown in the insert box). For comparison, the evolution of magnitude estimate provided by the JMA early warning system is also shown as a dotted gray line, and the continuous gray line represents the real moment magnitude value. (b) Real-time estimates of L_{10} (lilac filled circles) and L_{90} (purple empty circles) as provided by the slip inversion. Their running average and its error bar is also plotted (gray) for both parameters. (c) RMS error on intensity prediction (average value for the considered area). Light green filled circles show the RMS obtained using the current magnitude value from the inversion and assuming a point source (labeled as PS in the plot). Dark green empty circles show the RMS using the current magnitude value from the inversion and the finite fault estimate (FF in the plot). (d) Warning timeline for the Tohoku-Oki earthquake showing when the GPS information is available with respect to the time at which the strongest shaking occurs in the Sendai and Tokyo regions and with respect to the JMA warnings.

found a systematic, significant improvement in the ground shaking prediction when the finite fault is used (labeled as FF in the plot), with respect to the case of the point source (PS in the plot). Starting from the very beginning, our shaking prediction clearly indicates that high-intensity values are expected along the entire coast, from the closest Sendai area to the faraway Tokyo region. At the same time, when the point source is used, the intensity is instead largely underestimated especially far away from the epicenter region. We found, however, that the highest intensity values ($>$ 5.5–6) along the coast are not well reproduced. This may probably be due to the fact that we did not consider any local/site effect which may strongly affect the ground shaking.

4.2. The 2003 M_w 8.3 Tokachi-Oki Earthquake

[33] The 2003 M_w 8.3 Tokachi-Oki earthquake occurred on 25 September at 19:50:07 UTC along the Japan-Kuril trench off the Tokachi district of Hokkaido, northern Japan, where the Pacific Plate is subducting beneath the Hokkaido peninsula. Finite fault models indicate a thrust-fault mechanism (strike 234°, dip 7°, and rake 103°) rupturing an area of approximately 140×160 km with an estimated seismic moment of 2.9×10^{21} Nm [*Honda et al.*, 2004]. High coseismic displacements (up to 1 m) were recorded at the coastal stations of GEONET nearest the epicenter [*Honda et al.*, 2004; *Miura et al.*, 2004] where a permanent displacement of about 0.5 m has been observed [*Crowell et al.*, 2009]. Ground deformations were observed up to 200 km away from the source where the displacement amplitude exceeded 2 cm [*Irwan et al.*, 2004]. The analyzed data set consists of 169 three-component recording stations of the Japanese GPS Earth Observation Network (GEONET) [*Sagiya*, 2004], in a distance range between 80 and 600 km from the hypocenter. For this earthquake, we use a subduction interface with strike and dip of 211° and 11°, respectively, based on the USGS slab model for the subduction zone catalog of the Hokkaido, Japan region (http://earthquake.usgs.gov/research/data/slab/). Again, the fault is positioned to intersect the earthquake hypocenter and we assume a pure dip-slip reverse fault mechanism.

[34] The GPS strategy starts with the first trigger declaration 24 s after the origin time at the closest station (station 0134); the static offset extraction begins 10 s later, and the initial M_{NFPS} is 8.17. The starting fault plane is made with seven rectangular patches of 83×55 km each. Since the magnitude does not change significantly, the fault model size is not updated. The results are summarized in Figure 4 for three different times [24 s (Figure 4d), 100 s (Figure 4e), and 160 s (Figure 4f)] and shown in completeness in Figure S2 in the supporting information.

[35] For this M_w 8.3 earthquake, the initial M_{NFPS} and M_{FF} estimates are somewhat different being M_{NFPS} 8.17 and M_{FF} 8.45. The M_{NFPS} remains approximately constant to its initial value over the entire time range. The M_{FF} estimates vary between 8.15 and 8.45, starting high, and reaching a stable value ($M_{FF} = 8.2$) around 40 s from the origin time (Figure 5a). The estimated total length (L_{10}) has a stable mean value of 294 ± 26 km (varying between 228 and 355 km) (Figure 5b). The maximum slip area (L_{90}) ranges between 25 and 180, with a mean value of 74 ± 28 km (Figure 5b). Different finite fault models have been proposed for the 2003, Tokachi-Oki earthquake [*Honda et al.*, 2004;

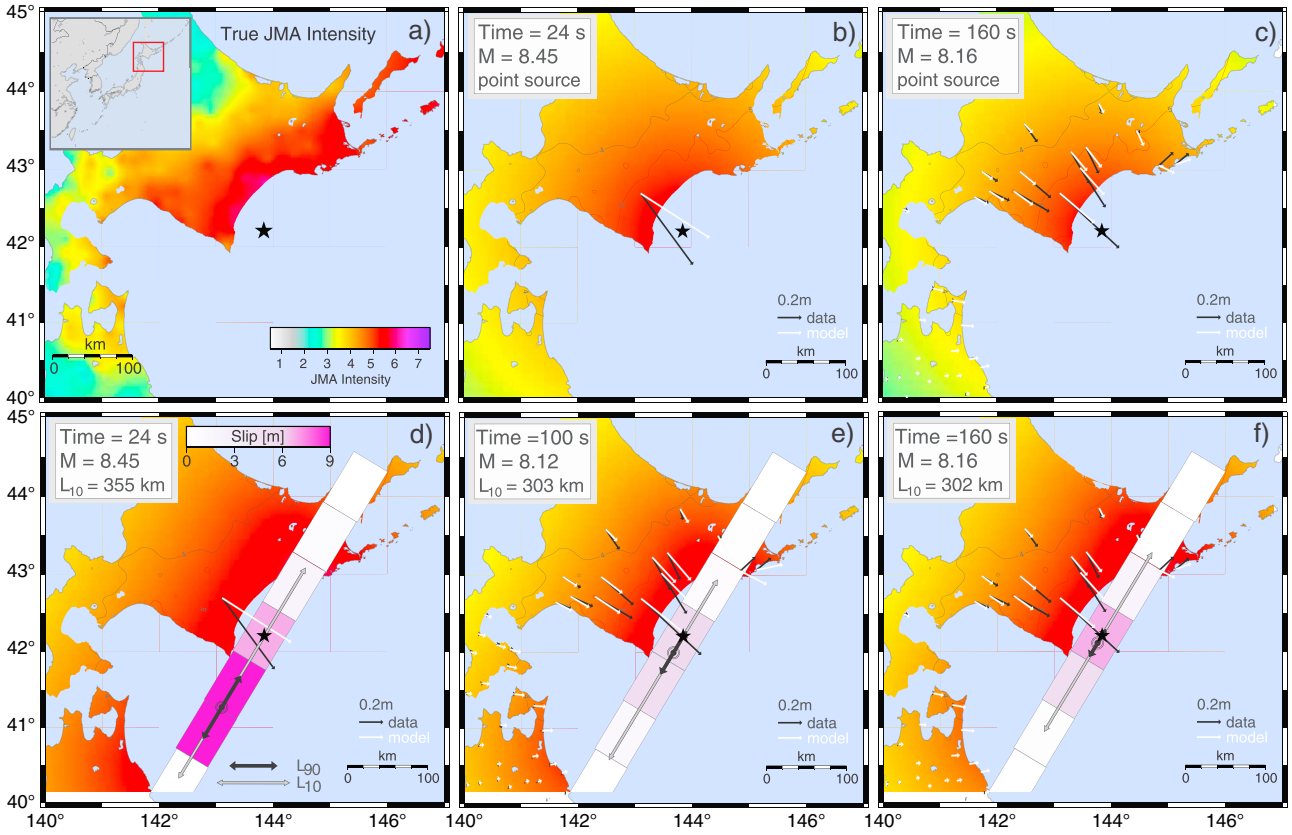

Figure 4. Snapshots of the GPS-based strategy inversion for the M_w 8.3, 2003 Tokachi-Oki earthquake at three different times comparing the (a) observed intensity with the predicted intensity using (b, c) the point source and (d, e, and f) the finite fault. The first result from the slip inversion is available 24 s (Figures 4b and 4d) after the origin time, followed by the estimates after 100 s (Figure 4e) and 160 s (Figures 4c and 4f). The corresponding predicted intensity distribution using the point source and the finite fault is shown as a background color. For details, refer to the caption of Figure 2.

Koketsu et al., 2004; *Romano et al.*, 2010]. The fault plane is generally modeled with an aspect ratio close to one (140 × 160 km, 120 × 100 km, and 210 × 150 km are examples of the adopted dimensions). A general feature resulting from the slip inversions is that the main asperity (with a peak slip of about 6 m) is concentrated in the northwest part of the fault plane and another ruptures area extends downdip from the hypocenter. While our real-time estimate of the total rupture length (L_{10}) is overestimated when compared to these postevent models, the area where most of the slip occurred is rather well approximated, in both extension (L_{90}) and position (centroid) on the plane.

[36] Due to the overestimation of the total rupture length, the ground shaking prediction for this earthquake is less accurate when the finite fault is considered compared to the use of a point source (Figure 5c). This is especially true at the initial seconds when the magnitude value is also overestimated. As the magnitude estimation decreases, the RMS gradually reaches an approximately stable value (~0.9) which is, however, still larger than the RMS obtained with the point source (~0.7). We return to this overestimation in section 5.

4.3. The M_w 7.2 El Mayor-Cucapah Earthquake

[37] The M_w 7.2, 2010 El Mayor-Cucapah earthquake occurred on 4 April 2010 at 22:40:42 UTC approximately

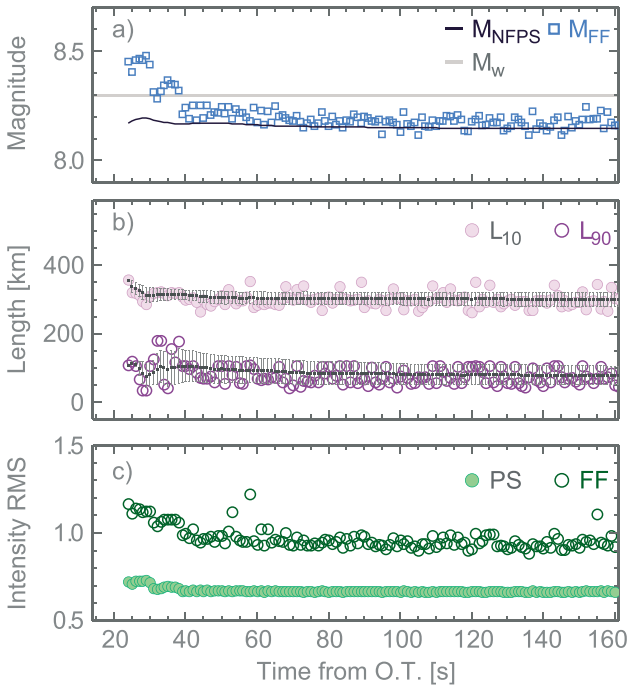

Figure 5. Real-time output for the M_w 8.3, 2003 Tokachi-Oki earthquake. For details, refer to the caption of Figure 3.

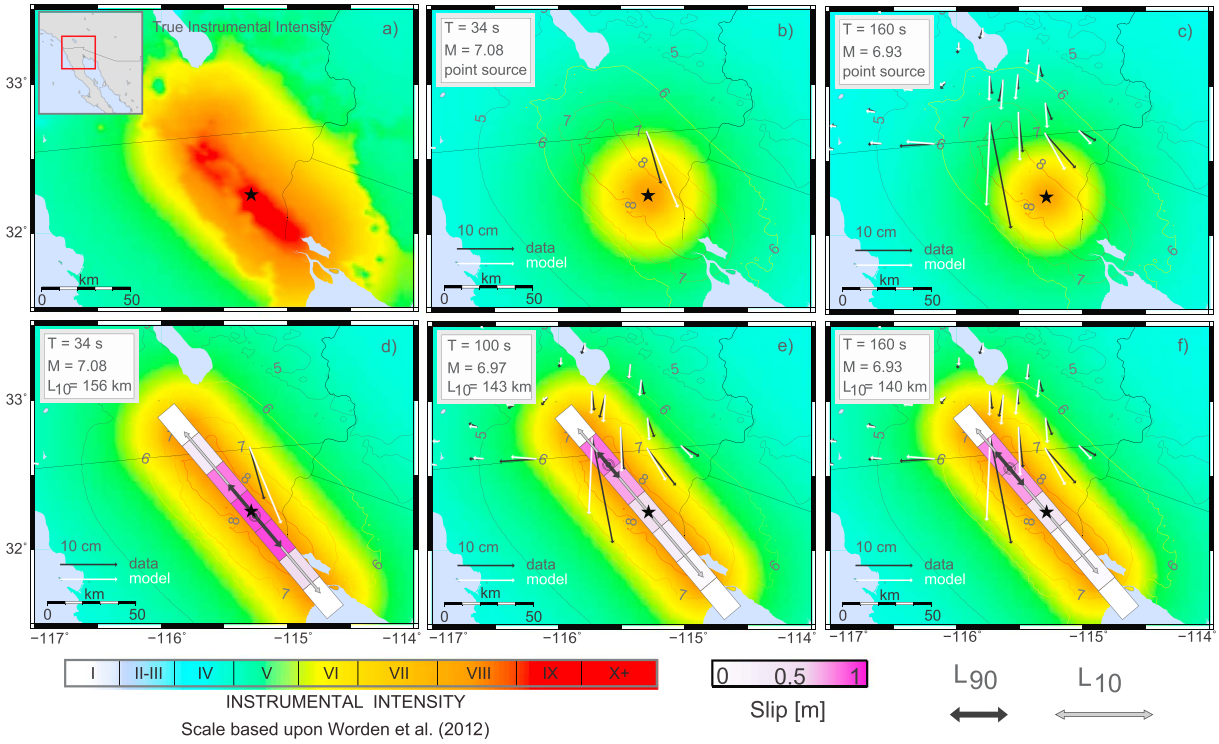

Figure 6. Snapshots of the GPS-based strategy inversion for the M_w 7.2, 2010 El Mayor-Cucapah earthquake at three different times comparing the (a) observed intensity with the predicted intensity using (b, c) the point source and (d, e, and f) the finite fault. The first result from the slip inversion is available 34 s (Figures 6b and 6d) after the origin time followed by the estimates after 100 s (Figure 6e) and 160 s (Figures 6c and 6f). The corresponding predicted intensity distribution using the point source and the finite fault is shown as a background color. The gray, yellow, orange, and red foreground lines represent the MMI = 5, 6, 7, and 8 contour lines, respectively. For details, refer to the caption of Figure 2.

50 km south of the Mexico-USA border along the boundary between the Pacific Plate and the North America Plate in northern Baja California. The main shock ruptured a series of fault segments with NW-SE alignment with a total extent of approximately 120 × 20 km and with an estimated seismic moment of about 3×10^{19} Nm [*Hauksson et al.*, 2010]. Moment tensor solutions and postearthquake imaging of the rupture process show evidence for a complex rupture history, with a dominant right-lateral strike-slip component (strike 234°, dip 7°, and rake 103°) combined with a significant nondouble-couple component [*Hauksson et al.*, 2010; *Wei et al.*, 2011]. We analyzed the coseismic displacement registered at 1 Hz GPS stations of the California Real-Time Network (CRTN). We model the fault plane with a pure vertical right-lateral strike-slip fault, striking at 320° and intersecting the earthquake hypocenter.

[38] We are able to detect the first trigger 34 s after the earthquake origin time at the station P494, where, 10 s later, the first estimation of static offset becomes available. Based on the first M_{NFPS} value ($M_{\mathrm{NFPS}} = 7.25$), we model the initial fault plane with seven rectangular patches of 28 × 16 km. Figure 6 shows the slip distribution obtained after 34 s (Figure 6d), 100 s (Figure 6e), and 160 s (Figure 6f), while the entire slip evolution is shown in Figure S3 in the supporting information.

[39] For this earthquake, we found very robust magnitude estimations both from M_{NFPS} and from M_{FF}. The two magnitudes are consistent with the M_w value for this event (M_w 7.2), although the magnitude resulting from the inversion shows a systematic small underestimation (about 0.2 magnitude units) with respect to M_{NFPS}. Specifically, M_{NFPS} ranges between 7.16 and 7.27, with a mean value of 7.2 while M_{FF} varies between 6.9 and 7.1, with a mean value around 7.0 (Figure 7a). L_{10} and L_{90} are also quite stable: L_{10} varies between 107 and 160 km, with a mean value over the entire time period of 143 ± 11 km, while L_{90} ranges between 10 and 62 km, with a mean value of 38 ± 14 km (Figure 7b).

[40] From the joint analysis of geodetic, remote-sensing and seismological data, *Wei et al.* [2011] reconstructed the fault geometry and the history of slip during the 2010 El Mayor-Cucapah earthquake. Their fault plane extended about 120 km along strike and about 20 km in the downdip direction. A similar result has been found by *Rodríguez-Pérez et al.* [2012] that, based on the distribution of aftershocks, modeled the fault plane as a rectangular area of 140 × 30 km. Most of the slip occurred in an area of approximately 40 × 10 km, concentrated in the northwestern part of the fault plane, where the rupture, after nucleating from the hypocenter, propagated and broke the largest asperity (Figure 3 from *Wei et al.* [2011]; Figure 4 from *Rodríguez-Pérez et al.* [2012]). Our real-time estimates of L_{10} and L_{90} show an excellent agreement with both the total length of the rupture area and the extension of the main asperity, respectively. The position of our real-time slip centroid also reproduces the observed northwest oriented slip distribution.

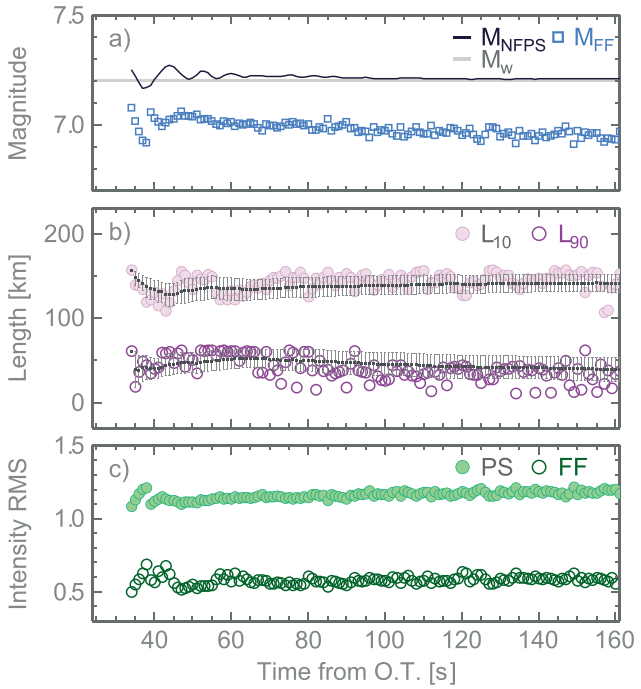

Figure 7. Real-time output for the M_w 7.2, 2010 El Mayor-Cucapah earthquake. For details, refer to the caption of Figure 3.

[41] In terms of ground shaking prediction, the El Mayor-Cucapah earthquake is the clearest evidence of how the prediction improves when the extended fault is considered. A visual comparison between the maps of Figure 6 shows that when the point source is used, the resulting intensity is biased, especially along the strike direction. When the extended fault plane is used, instead, a more realistic and accurate prediction of the intensity distribution is obtained. The RMS error on intensity (Figure 7c) is significantly reduced from a value of ~1.1 (with the point source) to ~0.6 when the finite fault is considered and remains approximately stable for the entire duration of the event.

5. Discussion

[42] In a real-time methodology for EEW, magnitude estimation has a key and fundamental role both for the rapid characterization of the event size and for a correct evaluation of the expected ground shaking at target sites. The proposed methodology based on the use of 1 Hz GPS displacement data provides a reasonable magnitude estimate for the three analyzed cases. This result is even more relevant when comparing the GPS-based magnitude to the seismic-based magnitude, the GPS-based estimates being significantly better (higher) than the real-time seismic-based estimates.

[43] In standard seismic approaches to EEW, the amplitude and/or frequency characteristics of the early recorded *P* wave signals are used to rapidly characterize the earthquake size. The 2011 megathrust Tohoku-Oki event has revealed that these methodologies may fail or saturate in case of very large and complex earthquakes. *Colombelli et al*. [2012] showed that the problem of magnitude saturation may be overcome by progressively expanding the *P* wave observation time window and including stations far away from the source. However, for the specific case of the Tohoku-Oki earthquake, the real-time data processing together with the frequency-dependent rupture process prevented determination of the correct event magnitude, and only allowed capture of the high-frequency radiation contribution of the first rupture episode.

[44] In contrast, for the same event, the GPS magnitude estimate is robust, and its time evolution reflects the complexity of the rupture process at the source. The first magnitude estimate ($M_{FF} = 8.15$) can be determined 39 s after the origin time. At the same time, the JMA magnitude was 7.6. Figure 3d shows the timeline for the Tohoku-Oki event, including when the GPS-based magnitude estimates are available with respect to the arrival of the strongest shaking. During the 2011, Tohoku-Oki earthquake, the epicenter was about 120 km offshore, and it took more than a minute before the strong motion arrived along the Sendai coast and nearly 2 minutes for the strongest shaking to hit residential areas in the Tokyo region. Our magnitude estimates could have been used for the prompt activation of emergency actions in the faraway Tokyo region as well as along the closest Sendai coast.

[45] For smaller earthquakes, around magnitude 7 such as the El Mayor-Cucapah, *Allen and Ziv* [2011] showed that magnitude estimation from GPS data is similar to the true moment magnitude obtained with seismic data from the beginning of the GPS strategy. This result is confirmed here and suggests that the proposed GPS-based strategy could be used to get independent magnitude estimates to confirm, or counter, the information released by seismic methodologies.

[46] In addition to the magnitude estimate, the proposed GPS methodology provides a real-time estimate of the rupture area extent, based on the slip distribution on the fault plane. Comparison of our inversion results with other postearthquake studies of detailed slip distribution shows that L_{10} and L_{90} are approximate, but useful estimates of the total rupture length and of the region where most of the slip is occurring, respectively. As with the magnitude, the fault length estimates (L_{10} and L_{90}) generated by this methodology are very stable in time. Having a stable real-time estimates of the rupture extent allows for estimation of the ground shaking intensity due to the finite source. This information should be integrated in a real-time EEW system to improve the ground shaking prediction by using the distance to the finite fault rather than distance from the hypocenter when estimating shaking intensity. This is the approach currently used by ShakeMap.

[47] For the 2011, M_w 9.0 Tohoku-Oki and the 2010, M_w 7.2 El Mayor-Cucapah earthquakes, we found a clear improvement in the intensity prediction when the real-time GPS magnitude estimates and the finite fault are considered. The intensity prediction is not as good in the case of the 2003 Tokachi-Oki earthquake. For Tokachi-Oki, the fault plane has been modeled by others with an aspect ratio close to one and a significant slip contribution comes from the deeper part of the plane. The downdip length of the fault planes are typically 2–3 times that of our model based on *Wells and Coppersmith* [1994] relations. The fact that we do not consider downdip variations in slip is indeed a limitation and is the main cause of our overestimate of the total rupture length (L_{10}) in this case. Adding a second row of slip patches in the inversion would likely improve our result in this case

as it would allow us to distinguish slip contributions from the downdip part of the fault. The absence of constraints adjacent to the fault between Hokkaido and the main island is also another reason for the overestimate of the total rupture area both at the first inversion and for the entire duration of the earthquake rupture (Figures 4d, 4e, and 4f). A possible solution could be to use a single patch model when only one data is available and then increase the number of patches, as more data become available, so to limit the number of unknowns parameters to less than the number of observations. With such an approach, estimating the length of the fault from the slip distribution would not be possible, and inverting for the slip on a fixed single patch would provide little more information than the point source magnitude estimate. A different strategy would be to allow the size of the patch to be solved for by the inversion, but this would again increase the number of free parameters to be determined.

[48] One of the assumptions that we make in the methodology is that the earthquake is occurring on a predefined fault plane, i.e., that we can extract from some catalog, and that there is very simple predefined rupture type, i.e., pure dip slip or strike slip depending on the tectonic environment. To assess the significance of this assumption, we simulated the real-time methodology for the Tohoku-Oki earthquake with a modified fault model, whose orientation differs from the previous case with a change in strike and dip of 15° and a change in rake of 20° (we used: strike = 180°; dip = 30°, rake = 70°, and depth = 20 km) (Figure S4 in the supporting information). This is intended to simulate the situation where the catalog fault geometry is only an approximation to the true geometry. We found that moderate changes in the orientation of the fault like this do not lead to significant differences in the estimated magnitude and slip distribution. A more serious source of error is when a dip-slip earthquake on an unidentified fault occurs in a strike-slip environment. While most faults and earthquakes are consistent with their tectonic environment, there are always the unusual cases, such as the 2002, Denali, Alaska event [*Ebehart-Phillips et al*., 2003] or the Mount Diablo thrust fault in the middle of multiple strike-slip faults throughout the San Francisco Bay Area [*Jones et al*., 1994]. Our methodology would most likely fail in this circumstance. For this reason, it would be prudent to define an acceptance criterion that must be met before the finite fault solution is used as part of an earthquake alert. One option might be to simultaneously solve for slip on different fault models (i.e., for strike-slip and dip-slip faults) and then let the RMS fit to the GPS data select the best fault model. The underestimate/overestimate of the GPS data can also provide a measure of whether the fault geometry, rake, or location is reasonable. Falling back on the point source-based earthquake alert is always an option for an early warning system.

[49] In the proposed methodology, the initial fault extent is defined based on the preliminary M_{NFPS}, and this may represent a possible source of error. We evaluated this effect by simulating an underestimated initial magnitude. We performed this test on the Tohoku-Oki earthquake, which is undoubtedly the most complex rupture event in our data set by simply assuming that the initial M_{NFPS} was 6.0 and seeing how the self-adapting strategy responded (Figure S5 in the supporting information). After a few underestimated initial solutions (small magnitude and short lengths), the magnitude rapidly increases (in 4–5 s) while ~25 s are necessary for the methodology to expand the fault plane and recover a length very similar to that shown in Figures 2 and 3.

[50] For the three analyzed earthquakes, we found a small, but systematic magnitude underestimation with respect to the moment magnitude (between 0.1 and 0.3). We identified several possible sources of this underestimation. One important factor is the smoothing filter applied to the slip distribution in the inversion step. This is necessary to avoid discontinuous and rough slip distributions but reduces the maximum slip value. Imprecise slip distributions also result from our simplified geometries and rupture types as well as from a coarse fault plane discretization. Finally, poor azimuthal station coverage is also a critical issue for all three earthquakes considered. For the case of the Tohoku-Oki earthquake, for example, due to the lack of stations along the plate boundary, the sensitivity to slip in the shallower part of the fault plane is very weak. Similarly, for El Mayor-Cucapah earthquake, the station position and geometry, with respect to the fault plane, provide a poor slip resolution in the extreme southeastern part of the plane. Still, the magnitude estimates that the methodology provides are remarkably accurate considering the simplicity of the approach, and a simple approach is more robust for application in an automated real-time setting.

6. Conclusion

[51] We investigated the possibility of using 1 Hz GPS data for earthquake early warning and developed an efficient methodology for both the rapid characterization of the earthquake magnitude and of the rupture area extent, using a real-time static slip inversion scheme. The strategy we propose does not require restrictive prior assumptions about the ongoing earthquake and is a "self-adapting" strategy, in which the initial fault plane to be used for the inversion is built based on a quick preliminary magnitude estimation, and the model is then upgraded as new magnitude values result from the slip inversion. In terms of early warning output, we deliver the real-time magnitude value, the estimated total length of the rupture area, and the length of the maximum slip area. The approximate position of the centroid of the slip distribution is also provided.

[52] To test and validate the proposed methodology, we applied the strategy to three different earthquakes: the M_w 9.0, 2011 Tohoku-Oki earthquake, the M_w 8.3, 2003 Tokachi-Oki earthquake, and the M_w 7.2, 2010 El Mayor-Cucapah earthquake. The first two events are in a subduction zone, and the third one occurred in a strike-slip environment. In principle, there is no limitation to the practical applicability of the proposed methodology to other tectonic environments, and no specific source-receiver configuration is required. As long as a good coverage and density of real-time GPS stations is available, the methodology is expected to be suitable for any seismically active area.

[53] For each analyzed event, we found a robust magnitude estimation that was significantly more accurate than the early real-time seismic-based estimates, particularly for the largest events. Encouraging results come from the rupture length estimation as well. A qualitative comparison of our results with postevent slip distribution models shows that L_{10} roughly corresponds to the observed total rupture length, and L_{90} approximately matches with the region where most of the slip has occurred. When estimating the shaking intensity using

ground motion prediction equations, we find that these predictions are improved using the GPS-based techniques as (1) the early magnitude estimate is improved over seismic methods, and (2) the shaking can be estimated as a function of distance to the fault rupture rather than distance to the hypocenter.

[54] As an illustration of the importance of assessing the finite extent of the fault, we can look to the warning issued for the 11 March 2011 M_w 9.0 Tohoku-Oki earthquake. The JMA warning system issued a warning before the *S* wave arrived onshore along the coast of Sendai. However, due to the magnitude underestimation and the use of a point source solution, they underestimated the shaking intensity for Tokyo and did not issue a public/cell phone warning. The real-time shaking estimates provided by our methodology for Tokyo are significantly higher due to the higher magnitude estimate and the use of a finite source. In addition to improvements in the accuracy of earthquake warnings for large events, this GPS-based finite source approach can also aid in tsunami warnings as the GPS-based magnitude estimates are available more rapidly than seismic-based methods.

[55] Finally, regarding the practical applicability of GPS-based methodology, there are currently a limited number of areas where real-time GPS networks are available. Real-time GPS sensors are operating in the United States (a partial list of available real-time networks can be found here: http://water.usgs.gov/osw/gps/real-time_network.html), and the Geographical Survey Institute in Japan has established a GPS permanent observation station network (GEONET) covering all of the Japanese islands with about 1000 observation sites. In Italy, a network of several permanent (not yet real-time) GPS stations of the Italian National Institute of Geophysics and Volcanology has been in development since 2006. While the number of locations where our real-time methodology can be applied is limited today, the value of continuous and real-time GPS networks is becoming clear, and we therefore anticipate rapid expansion.

[56] **Acknowledgments.** For the 2011 Tohoku-Oki earthquake, raw 1 Hz GPS data were collected by the Japanese GPS Earth Observation Network (GEONET) [*Sagiya*, 2004], and point positions were provided by the Pacific Northwest Geodetic Array at Central Washington University and were computed using GIPSY 6 and final satellite ephemerides and clock corrections provided by the Jet Propulsion Laboratory. For the 2003 Tokachi-Oki earthquake, raw 1 Hz GPS data was collected by the GEONET network and was postprocessed using the method of instantaneous positioning described in *Bock et al*. [2011]. For the 2010 El Mayor-Cucapah earthquake, the GPS displacement waveforms were postprocessed using the method of instantaneous positioning described in *Bock et al*. [2011], and are a product of the ASA AIST project (grant NNX09AI67G) at Scripps, JPL, and Caltech, and were obtained from SCEDC (http://www.data.scec.org/research/MayorCucapah20100404/). Raw GPS data used in the computation of the displacement waveforms were provided by the Southern California Integrated GPS Network and its sponsors, the W. M. Keck Foundation, NASA, NSF, USGS, and SCEC. For this study, the displacement waveforms were stored and analyzed in SAC format [*Goldstein et al*., 2003]. All figures and individual frames of animations were created using the GMT software [*Wessel and Smith*, 1995], and a MATLAB code was used for the inversion procedure (MATLAB version 6.5.1, 2003, computer software, The MathWorks Inc., Na tick, Massachusetts). This work was funded by the University of Naples Federico II, the University of Bologna Alma Mater Studiorum, and a grant to UC Berkeley from the Gordon and Betty Moore Foundation. This research was carried out in the framework of REAKT Project (Strategies and tools for Real-Time EArthquake RisK ReducTion) founded by the European Community via the Seventh Framework Program for Research (FP7), contract 282862. Manoocheer Shrirzaei has provided invaluable assistance during this work and we wish to thank Douglas Dreger and Roland Bürgmann for their precious and constructive comments. We are grateful to Anthony Lomax and David Schmidt for their comments about our work and for the care with which they reviewed our manuscript.

References

Aki, K., and G. P. Richards (2002), *Quantitative Seismology*, 2nd ed., University Science Book, Sausalito, Calif.

Alcik, H., O. Ozel, N. Apaydin, and M. Erdik (2009), A study on warning algorithms for Istanbul earthquake early warning system, *Geophys. Res. Lett.*, *36*, L00B05, doi:10.1029/2008GL036659.

Allen, R. V. (1978), Automatic earthquake recognition and timing from single traces, *Bull. Seismol. Soc. Am.*, *68*, 1521–1532.

Allen, R. M., and H. Kanamori (2003), The potential for earthquake early warning in Southern California, *Science*, *3*, 685–848.

Allen, R. M., and A. Ziv (2011), Application of real-time GPS to earthquake early warning, *Geophys. Res. Lett.*, *38*, L16310, doi:10.1029/2011GL047947.

Allen, R. M., H. Brown, M. Hellweg, O. Khainovski, P. Lombard, and D. Neuhauser (2009a), Real-time earthquake detection and hazard assessment by ElarmS across California, *Geophys. Res. Lett.*, *36*, L00B08, doi:10.1029/2008GL036766.

Allen, R. M., P. Gasparini, O. Kamigaichi, and M. Böse (2009b), The status of earthquake early warning around the world: An introductory overview, *Seismol. Res. Lett.*, *80*, 682–693.

Anzidei, M., et al. (2009), Coseismic deformation of the destructive April 6, 2009 L'Aquila earthquake (central Italy) from GPS data, *Geophys. Res. Lett.*, *36*, L17307, doi:10.1029/2009GL039145.

Avallone, A., M. Marzario, A. Cirella, A. Piatanesi, A. Rovelli, C. Di Alessandro, E. D'Anastasio, N. D'Agostino, R. Giuliani, and M. Mattone (2011), Very high rate (10 Hz) GPS seismology for moderate magnitude earthquakes: The case of the Mw 6.3 L'Aquila (central Italy) event, *J. Geophys. Res.*, *116*, B02305, doi:10.1029/2010JB007834.

Bock, Y., L. Prawirodirdjo, and T. I. Melbourne (2004), Detection of arbitrarily large dynamic ground motions with a dense high-rate GPS network, *Geophys. Res. Lett.*, *31*, L06604, doi:10.1029/2003GL019150.

Bock, Y., D. Melgar, and B. W. Crowell (2011), Real-time strong-motion broadband displacements from collocated GPS and accelerometers, *Bull. Seismol. Soc. Am.*, *101*, 2904–2925, doi:10.1785/0120110007.

Boore, D. M., W. B. Joyner, and T. E. Fumal (1997), Equations for estimating horizontal response spectra and peak acceleration from western North American earthquakes: A summary of recent work, *Seismol. Res. Lett.*, *68*(1), 128–153.

Boore, D. M., C. D. Stephens, and W. B. Joyner (2002), Comments on baseline correction of digital strong-motion data: Examples from the 1999 Hector Mine, California, earthquake, *Bull. Seismol. Soc. Am.*, *92*, 1543–1560, doi:10.1785/0120000926.

Böse, M., C. Ionescu, and F. Wenzel (2007), Earthquake early warning for Bucharest, Romania: Novel and revised scaling relations, *Geophys. Res. Lett.*, *34*, L07302, doi:10.1029/2007GL029396.

Böse, M., E. Hauksson, K. Solanki, H. Kanamori, and T. H. Heaton (2009), Real-time testing of the on-site warning algorithm in Southern California and its performance during the July 29, 2008 Mw 5.4 Chino Hills earthquake, *Geophys. Res. Lett.*, *36*, L00B03, doi:10.1029/2008GL036366.

Brown, H., R. M. Allen, and V. Grasso (2009), Testing ElarmS in Japan, *Seismol. Res. Lett.*, *80*, 727–739, doi:10.1785/gssrl.80.5.727.

Cirella, A., A. Piatanesi, M. Cocco, E. Tinti, L. Scognamiglio, A. Michelini, A. Lomax, and E. Boschi (2009), Rupture history of the 2009 L'Aquila (Italy) earthquake from non-linear joint inversion of strong motion and GPS data, *Geophys. Res. Lett.*, *36*, L19304, doi:10.1029/2009GL039795.

Colombelli, S., A. Zollo, G. Festa, and H. Kanamori (2012), Early magnitude and potential damage zone estimates for the great Mw 9 Tohoku-Oki earthquake, *Geophys. Res. Lett.*, *39*, L22306, doi:10.1029/2012GL053923.

Crowell, B. W., Y. Bock, and M. B. Squibb (2009), Demonstration of earthquake early warning using total displacement waveforms from real-time GPS networks, *Seismol. Res. Lett.*, *80*, 772–782, doi:10.1785/gssrl.80. 5.772.

Crowell, B. W., Y. Bock, and D. Melgar (2012), Real-time inversion of GPS data for finite fault modeling and rapid hazard assessment, *Geophys. Res. Lett.*, *39*, L09305, doi:10.1029/2012GL051318.

Ebehart-Phillips, D., et al. (2003), The 2002 Denali Fault earthquake, Alaska: A large magnitude, slip-partitioned event, *Science*, *300*, 1113–1118, doi:10.1126/science.1082703.

Espinosa-Aranda, J. M., A. Cuellar, A. Garcia, G. Ibarrola, R. Islas, S. Maldonado, and F. H. Rodriguez (2009), Evolution of the Mexican Seismic Alert System (SASMEX), *Seismol. Res. Lett.*, *80*, 694–706.

Genrich, J. F., and Y. Bock (2006), Instantaneous geodetic positioning with 10–50 Hz GPS measurements: Noise characteristics and implications for monitoring networks, *J. Geophys. Res.*, *111*, B03403, doi:10.1029/2005JB003617.

Goldstein, P., D. Dodge, M. Firpoand, and L. Minner (2003), SAC2000: Signal processing and analysis tools for seismologists and engineers, in *IASPEI International Handbook of Earthquake and Engineering Seismology*, pp. 1613–1614, edited by W. H. K. Lee, H. Kanamori, P. C. Jennings, and C. Kisslinger, Elsevier, New York.

Hanks, T., and H. Kanamori (1979), A moment magnitude scale, *J. Geophys. Res.*, *84*, 2348–2350, doi:10.1029/JB084iB05p02348.

Hauksson, E., J. Stock, K. Hutton, W. Yang, A. Vidal, and H. Kanamori (2010), The 2010 Mw 7.2 El Mayor-Cucapah earthquake sequence, Baja California, Mexico and southernmost California, USA: Active seismotectonics along the Mexican Pacific margin, *Pure Appl. Geophys.*, *168*, 1255–1277, doi:10.1007/s00024-010-0209-7.

Holland, J. H. (1975), *Adaptation in Natural and Artificial Systems*, Univ. of Mich. Press, Ann Arbor.

Holland, J. H. (1992), Genetic algorithms, *Sci. Am.*, *267*, 66–72.

Honda, R., S. Aoi, N. Morikawa, H. Sekiguchi, T. Knugi, and H. Fujiwara (2004), Ground motion and rupture process of the 2003 Tokachi-Oki earthquake obtained from strong motion data of K-net and KiK-net, *Earth Planets Space*, *56*, 317–322.

Horiuchi, S., N. Negishi, K. Abe, K. Kamimura, and Y. Fujinawa (2005), An automatic processing system for broadcasting system earthquake alarms, *Bull. Seismol. Soc. Am.*, *95*, 347–353.

Iinuma, T., et al. (2011), Coseismic slip distribution of the 2011 off the Pacific Coast of Tohoku Earthquake (M9.0) refined by means of seafloor geodetic data, *J. Geophys. Res.*, *117*, B07409, doi:10.1029/2012JB009186.

Irwan, M., F. Kimata, K. Hirahara, T. Sagiya, and A. Yamagiwa (2004), Measuring ground deformation with 1-Hz GPS data: The 2003 Tokachi-Oki earthquake (preliminary report), *Earth Planets Space*, *56*, 389–393.

Jones, D. L., R. Graymer, C. Wang, T. V. McEvilly, and A. Lomax (1994), Neogene transpressive evolution of the California Coast Ranges, *Tectonics*, *13*, 561–574, doi:10.1029/93TC03323.

Joyner, W. B., and D. M. Boore (1981), Peak horizontal acceleration and velocity from strong-motion records including records from the 1979 Imperial Valley, California, earthquake, *Bull. Seismol. Soc. Am.*, *71*, 2011–2038.

Kanamori, H. (2005), Real-time seismology and earthquake damage mitigation, *Annu. Rev. Earth Planet. Sci.*, *33*, 195–214.

Kanamori, H., and E. Brodsky (2004), The physics of earthquakes, *Rep. Prog. Phys.*, *67*, 1429–1496.

Kinoshita, S., and M. Takagishi (2011), Generation and propagation of static displacement estimated using KiK-net recordings, *Earth Planets Space*, *63*, 779–783, doi:10.5047/eps.2011.05.003.

Koketsu, K., K. Hikima, S. Miyazaki, and I. Satoshi (2004), Joint inversion of strong motion and geodetic data for the source process of the 2003 Tokachi-Oki, Hokkaido, earthquake, *Earth Planets Space*, *55*, 329–334.

Langbein, J., and Y. Bock (2004), High-rate real-time GPS network at Parkfield; utility for detecting fault slip and seismic displacements, *Geophys. Res. Lett.*, *31*, L15S20, doi:10.1029/2003GL019408.

Larson, K. M., P. Bodin, and J. Gomberg (2003), Using 1-Hz GPS data to measure deformations caused by the Denali Fault Earthquake, *Science*, *300*, 1421–1424.

Lee, S. J., B. S. Huang, M. Ando, H. C. Chiu, and H. J. Wang (2011), Evidence of large scale repeating slip during the 2011 Tohoku-Oki earthquake, *Geophys. Res. Lett.*, *38*, L19306, doi:10.1029/2011GL049580.

Midorikawa, S., K. Fujimoto, and I. Muramatsu (1999), Correlation of new J.M. A. instrumental seismic intensity with former J.M.A. seismic intensity and ground motion parameters [in Japanese], *J. Inst. Social Saf. Sci.*, *1*, 51–56.

Miura, S., Y. Suwa, A. Hasegawa, and T. Nishimura (2004), The 2003 M8.0 Tokachi-Oki earthquake: How much has the great event paid back slip debts?, *Geophys. Res. Lett.*, *31*, L05613, doi:10.1029/2003GL019021.

Nakamura, Y. (1984), Development of earthquake early-warning system for the Shinkansen, some recent earthquake engineering research and practical in Japan, pp. 224–238, Jpn. Natl. Comm., Int. Assoc. for Earthquake Eng.

Nakamura, Y. (1988), On the urgent earthquake detection and alarm system (UrEDAS), in *Proceedings 9th World Conf. Earthquake Eng.*, 7, 673–678.

Odaka, T., K. Ashiya, S. Tsukada, S. Sato, K. Ohtake, and D. Nozaka (2003), A new method of quickly estimating epicentral distance and magnitude from a single seismic record, *Bull. Seismol. Soc. Am.*, *93*, 526–532.

Ohta, Y., et al. (2012), Quasi real-time fault model estimation for near-field tsunami forecasting based on RTK-GPS analysis: Application to the 2011 Tohoku-Oki earthquake (Mw 9.0), *J. Geophys. Res.*, *117*, B02311, doi:10.1029/2011JB008750.

Okada, Y. (1985), Surface deformation due to shear and tensile faults in a half-space, *Bull. Seismol. Soc. Am.*, *75*, 1135–1154.

Peng, H. S., Z. L. Wu, Y. M. Wu, S. M. Yu, D. N. Zhang, and W. H. Huang (2011), Developing a prototype earthquake early warning system in the Beijing Capital Region, *Seismol. Res. Lett.*, *82*, 294–403.

Rodríguez-Pérez, Q., L. Ottemöller, and R. R. Castro (2012), Stochastic finite-fault ground-motion simulation and source characterization of the 4 April 2010 M_w 7.2 El Mayor-Cucapah Earthquake, *Seismol. Res. Lett.*, *83*, 235–249, doi:10.1785/gssrl.83.2.235.

Romano, F., A. Piatanesi, S. Lorito, and K. Hirata (2010), Slip distribution of the 2003 Tokachi-Oki M_w 8.1 earthquake from joint inversion of tsunami waveforms and geodetic data, *J. Geophys. Res.*, *115*, B11313, doi:10.1029/2009JB006665.

Romano, F., A. Piatanesi, S. Lorito, N. D'Agostino, K. Hirata, S. Atzori1, Y. Yamazaki, and M. Cocco (2012), Clues from joint inversion of tsunami and geodetic data of the 2011 Tohoku-Oki earthquake, *Sci. Rep.*, *2*, 385, doi:10.1038/srep00385.

Rydelek, P., and S. Horiuchi (2006), Is earthquake rupture deterministic?, *Nature*, *442*, E5–E6, doi:10.1038/nature04963.

Rydelek, P., C. Wu, and S. Horiuchi (2007), Comment on "Earthquake magnitude estimation from peak amplitudes of very early seismic signals on strong motion records" by Aldo Zollo, Maria Lancieri, and Stefan Nielsen, *Geophys. Res. Lett.*, L20302, *34*, doi:10.1029/2007GL029387.

Sagiya, T. (2004), A decade of GEONET: 1994–2003 The continuous GPS observation in Japan and its impact on earthquake studies, *Earth Planets Space*, *56*, xxix–xli.

Satriano, C., A. Lomax, and A. Zollo (2008), Real-time evolutionary earthquake location for seismic early warning, *Bull. Seismol. Soc. Am.*, *98*, 1482–1494, doi:10.1785/0120060159.

Satriano, C., L. Elia, C. Martino, M. Lancieri, A. Zollo, and G. Iannaccone (2010), PRESTo, the earthquake early warning system for southern Italy: Concepts, capabilities and future perspectives, *Soil Dyn. Earthquake Eng.*, *31*(2), 137–153, doi:10.1016/j.soildyn.2010.06.008.

Shieh, J. T., Y. M. Wu, and R. M. Allen (2008), A comparison of τ_c and τ_p^{max} for magnitude estimation in earthquake early warning, *Geophys. Res. Lett.*, *35*, L20301, doi:10.1029/2008GL035611.

Shirzaei, M., and T. R. Walter (2009), Randomly Iterated Search and Statistical Competency (RISC) as powerful inversion tools for deformation source modeling: Application to volcano InSAR data, *J. Geophys. Res.*, *114*, B10401, doi:10.1029/2008JB006071.

Si, H., and S. Midorikawa (1999), Attenuation relations for peak ground acceleration and velocity considering effects of fault type and site condition [in Japanese], *J. Struct. Construct. Eng.*, *523*, 63–70.

Simons, M., et al. (2011), The 2011 magnitude 9.0 Tohoku-Oki earthquake: Mosaicking the megathrust from seconds to centuries, *Science*, *332*, 1421–1425, doi:10.1126/science.1206731.

Suzuki, W., S. Aoi, H. Sekiguchi, and T. Kunugi (2011), Rupture process of the 2011 Tohoku-Oki mega-thrust earthquake (M9.0) inverted from strong motion data, *Geophys. Res. Lett.*, *38*, L00G16, doi:10.1029/2011GL049136.

Wei, S., et al. (2011), Superficial simplicity of the 2010 El Mayor-Cucapah earthquake of Baja California in Mexico, *Nat. Geosci.*, *4*, 615–618, doi:10.1038/ngeo1213.

Wells, D. L., and K. J. Coppersmith (1994), New empirical relationships among magnitude, rupture length, rupture width, rupture area, and surface displacement, *Bull. Seismol. Soc. Am.*, *84*, 974–1002.

Wessel, P., and W. H. F. Smith (1995), New version of the generic mapping tools released, *Eos Trans*, AGU, *76*, 329.

Worden, C. B., M. C. Gerstenberger, D. A. Rhoades, and D. J. Wald (2012), Probabilistic relationships between ground-motion parameters and modified mercalli intensity in California, *Bull. Seismol. Soc. Am.*, *102*(1), 204–221, doi:10.1785/0120110156.

Wright, T. J., N. Houlié, M. Hildyard, and T. Iwabuchi (2012), Real-time, reliable magnitudes for large earthquakes from 1 Hz GPS precise point positioning: The 2011 Tohoku-Oki (Japan) earthquake, *Geophys. Res. Lett.*, *39*, L12302, doi:10.1029/2012GL051894.

Wu, Y. M., and H. Kanamori (2008), Development of an earthquake early warning system using real-time strong motion signals, *Sensors*, *8*, 1–9.

Wu, Y. M., and T. L. Teng (2002), A virtual sub-network approach to earthquake early warning, *Bull. Seismol. Soc. Am.*, *92*, 2008–2018.

Wu, Y. M., and L. Zhao (2006), Magnitude estimation using the first three seconds P-wave amplitude in earthquake early warning, *Geophys. Res. Lett.*, *33*, L16312 doi:10.1029/2006GL026871.

Yamagiwa, A., Y. Hatanaka, T. Yutsudo, and B. Miyahara (2006), Real time capability of GEONET system and its application to crust monitoring, *Bull. Geogr. Surv.*, *53*, 27–33.

Zollo, A., M. Lancieri, and S. Nielsen (2006), Earthquake magnitude estimation from peak amplitudes of very early seismic signals on strong motion, *Geophys. Res. Lett.*, *33*, L23312 doi:10.1029/2006GL027795.

Zollo, A., M. Lancieri, and S. Nielsen (2007), Reply to comment by P. Rydelek et al., on "Earthquake magnitude estimation from peak amplitudes of very early seismic signals on strong motion records," *Geophys. Res. Lett.*, *34*, L20303, doi:10.1029/2007GL030560.

Zollo, A., et al. (2009), The earthquake early warning system in southern Italy, *Encycl. Complexity Syst. Sci.*, *5*, 2395–2421, doi:10.1007/978-0-387-30440-3.

Zollo, A., S. Colombelli, L. Elia, A. Emolo, G. Festa, G. Iannaccone, C. Martino, and P. Gasparini (2013), An integrated regional and on-site Earthquake Early Warning System for Southern Italy: Concepts, methodologies and performances, *in Early Warning for Geological Disasters, Scientific Concepts and Current Practice*, pp. 117–136, edited by Wenzel and Zschau, Springer, Berlin, Heidelberg, doi:10.1007/978–3–642–12233–0.